





Cite this: *RSC Adv.*, 2020, 10, 41462

Effects of chlorinated Pd precursors and preparation methods on properties and activity of Pd/TiO₂ catalysts†

Ye Eun Kim, ^{ab} Mi Yeon Byun,^{ac} Kwan-Young Lee ^{*b} and Man Sig Lee ^{*ad}

We investigated the effects of Pd precursors and preparation methods on the physicochemical properties and performance of Pd/TiO₂ catalysts in the photocatalytic degradation of methyl violet. To confirm the influence of the precursors, Pd/TiO₂ catalysts were prepared *via* chemical reduction (CR) using four different Pd precursors. Additionally, to determine the effects of preparation methods, Pd/TiO₂ catalysts were fabricated using K₂PdCl₄ precursor *via* three different methods: CR, deposition–precipitation (DP), and impregnation. The CO chemisorption results showed that the catalyst prepared *via* DP using the K₂PdCl₄ precursor, *i.e.*, Pd/TiO₂_K_DP, displayed the highest Pd dispersion of 12.42% owing to the stable formation of Pd(OH)₂, which strongly interacted with the –OH groups on the TiO₂ support. Although the catalyst prepared *via* CR using the Pd(NH₃)₄Cl₂·H₂O (PA) precursor, *i.e.*, Pd/TiO₂_PA_CR, had the lowest Pd dispersion of 0.7%, it exhibited the highest absorption of 26% after 30 min in the dark. It was found that high Pd²⁺/Pd⁰ ratio in dark conditions adversely affected the absorption of MV owing to electrostatic repulsion between the cationic dyes and metal nanoparticles. However, the Pd dispersion and the specific surface area played a key role in the photocatalytic activity under UV irradiation. Pd/TiO₂_K_CR with higher Pd dispersion showed the highest photocatalytic activity and reaction rate of 0.0212 min^{−1}.

Received 1st September 2020
Accepted 1st November 2020

DOI: 10.1039/d0ra07510h

rsc.li/rsc-advances

Introduction

Methyl violet, a cationic, basic, and hazardous dye, is extensively used in various industries.¹ Approximately 20% of the commercial dye used is discarded.² It is not removed *via* washing with water and causes water pollution. In general, only 80% of the dye molecules and chemical mixtures can be decolorized.³ Dye effluents are harmful to living beings and pose the risk of cancer to humans.⁴ Countless research papers have been published on biological, physical, and electrochemical methods for the successful removal of dye particles.^{5–7} Photocatalytic degradation of dye molecules is an efficient and environment-friendly process to remove organic pollutants and does not produce additional toxic by-products.

Photocatalysts are typically fabricated from semiconductors owing to their unique physical and chemical properties under

light irradiation. Among a wide range of semiconductors, TiO₂ has attracted significant attention owing to its high chemical and thermal stability, low cost, and non-toxicity. In recent reviews, the deposition of noble metals such as Ag, Au, Pd, and Pt was found to improve the photocatalytic performance significantly. Many studies have shown that Pd/TiO₂ exhibits higher photocatalytic activity compared with that of pristine TiO₂.^{8–10} Khojasteh *et al.* demonstrated that the metallic state further enhanced the photodegradation of rhodamine B owing to the creation of a Schottky barrier between Pd⁰ and TiO₂.¹¹ Wu *et al.* reported enhanced adsorption capacity of NO over Pd²⁺ modified on TiO₂.¹² Meng *et al.* reported that Pd²⁺ doped on semiconductors increased the photodegradation of rhodamine B by narrowing the band gap of the latter.¹³

Herein, we investigated the effects of four Pd precursors and three preparation methods on the Pd charge states and photocatalytic activity of the corresponding Pd/TiO₂ catalysts based on their photocatalytic degradation of methyl violet 2B (MV).

Experimental

Materials

Palladium(II) chloride (PdCl₂, 99.9%), palladium(II) nitrate hydrate (Pd(NO₃)₂·2H₂O, ≥99.0%), tetraamine palladium(II) chloride (Pd(NH₃)₄Cl₂·H₂O, 98%), hydrochloric acid (HCl solution, 38%), sodium chloride (NaCl, 99.9%), sodium tartrate

^aUlsan Division, Korea Institute of Industrial Technology (KITECH), Ulsan 44413, Republic of Korea. E-mail: lms5440@kitech.re.kr

^bDepartment of Chemical and Biological Engineering, Korea University, Seoul 02841, Republic of Korea. E-mail: kylee@korea.ac.kr

^cDepartment of Polymer Science and Chemical Engineering, Pusan National University, Busan 46241, Republic of Korea

^dDepartment of Green Process and System Engineering, University of Science and Technology (UST), Ulsan 44413, Republic of Korea

† Electronic supplementary information (ESI) available: Direct band gap calculation data. See DOI: 10.1039/d0ra07510h



($\text{Na}_2\text{C}_4\text{H}_4\text{O}_6$, $\geq 99.0\%$), sodium hydroxide (NaOH , 99.8%), sodium borohydride (NaBH_4 , 98.0%), and 5,5-dimethyl-pyrroline-*N*-oxide (DMPO) were purchased from Sigma Aldrich. Potassium tetrachloropalladate(II) (K_2PdCl_4 , 99.99%) and sodium formate (HCOONa , 99.0%) were purchased from Alfa Aesar. Commercial TiO_2 (P25) was purchased from Evonik Degussa.

Preparation of catalysts

The Pd precursors were prepared by dissolving 0.1 mol PdCl_2 in 0.2 M HCl solution or 0.2 M NaCl solution and 0.1 mol of K_2PdCl_4 , 0.1 mol $\text{Pd}(\text{NO}_3)_2 \cdot 2\text{H}_2\text{O}$, and 0.1 mol $\text{Pd}(\text{NH}_3)_4\text{Cl}_2 \cdot \text{H}_2\text{O}$ in distilled water.

A series of 5 wt% Pd/TiO_2 catalysts was prepared *via* chemical reduction (CR) using four different Pd precursors: H_2PdCl_4 (H), K_2PdCl_4 (K), Na_2PdCl_4 (N), and $\text{Pd}(\text{NH}_3)_4\text{Cl}_2 \cdot \text{H}_2\text{O}$ (PA). We then prepared Pd/TiO_2 catalysts using the precursor K *via* three different methods of preparation: CR, deposition–precipitation (DP), and impregnation (IM).

In the CR method, 5.64 mL of 0.1 M Pd precursor was suspended into 0.15 mmol $\text{Na}_2\text{C}_4\text{H}_4\text{O}_6$ in 150 mL of distilled water at 5 °C, following which 1.14 g of TiO_2 support was added. A 0.02 M NaOH solution was injected to adjust the pH value to 11 and the mixture was stirred for 2 h. Thereafter 30 mmol NaBH_4 in 100 mL of distilled water was injected to reduce the Pd^{2+} ions in the aqueous medium and the mixture was stirred for an additional 2 h. After reduction for 2 h, the solution was filtered, washed, and dried at 105 °C for 12 h.

In the DP method, 100 mL of distilled water was heated to 60 °C, following which 0.1 M K_2PdCl_4 was added and 1.14 g of TiO_2 support was suspended into the solution. Next, 0.25 M NaOH was added to the TiO_2 suspension to adjust the pH value to 11 for 3 h. Thereafter, 30 mmol HCOONa in 100 mL of distilled water was injected and the mixture was stirred for another 3 h. The solution was filtered, washed, and dried at 105 °C for 12 h.

In the IM method, 0.1 M K_2PdCl_4 in 50 mL of distilled water was stirred with 1.14 g of TiO_2 support for 1 h to impregnate the Pd precursor. After the excess water had evaporated, the impregnated catalysts were dried at 105 °C for 1 h, calcined in air at 400 °C for 4 h, and then heated at 200 °C for 2 h in a 4% H_2/N_2 flow.

The catalysts prepared were denoted by $\text{Pd}/\text{TiO}_2\text{-A}_i\text{-B}$ (A: Pd precursor, B: preparation method).

Catalyst characterization

To identify the phase compositions of the catalysts prepared, their X-ray diffraction (XRD) patterns were obtained using a D/MAX 2500-V/PC instrument (Rigaku, Japan) with $\text{Cu K}\alpha$ radiation. The 2θ scanning range was 10–80° at a scan rate of 5° min^{-1} . The physical properties of the support and the catalysts prepared were studied based on N_2 adsorption–desorption at 77 K using a Brunauer–Emmett–Teller (BET) apparatus on an ASAP 2020 instrument (Micromeritics, USA). Each sample was degassed under vacuum (<10 mm Hg) at 150 °C for 4 h before N_2 physisorption. Micropore volume was calculated by the

Horvath–Kawazoe (HK) method assuming slit pore geometry. To confirm the functional groups on the support and catalysts, Fourier transform infrared spectroscopy (FT-IR) was performed with a 1700 series FT-IR spectrometer (PerkinElmer, USA) in the 400–4000 cm^{-1} range using the KBr pellet method. The CO chemisorption measurements were carried out using an ASAP 2020 instrument (Micromeritics, USA) to identify the Pd dispersion and amount of CO adsorbed. The catalysts prepared were evacuated at 200 °C for 30 min and reduced in H_2 at 250 °C for 2 h. Subsequently, they were evacuated again at 250 °C for 2 h and then cooled to 35 °C. The temperature-programmed desorption of CO (CO-TPD) was performed using an AutoChem 2920 instrument (Micromeritics, USA). Approximately 0.1 g of each Pd/TiO_2 catalyst was placed in a reactor and CO (10% CO/He , 50 mL min^{-1}) was adsorbed at a heating rate of 5° min^{-1} as the temperature was increased from 40 °C to 500 °C. The Pd particle size and distribution were obtained using a JEM-2010 transmission electron microscope (JEOL, Japan) operated at 200 kV with an optical point-to-point resolution of 0.23 nm. The X-ray photoelectron spectroscopy (XPS) analyses were carried out using a K-Alpha⁺ instrument (Thermo Fisher Scientific, USA). The diffuse reflectance spectra were analyzed using an ultraviolet-visible light (UV-vis) spectrophotometer (Shimadzu, Japan) in the wavelength range 200–700 nm to calculate the band gap energies. BaSO_4 was used as the reference sample. The generation of the reactive oxygen species (ROS) was observed by the JES-TE200 electron spin resonance (ESR, JEOL, Japan). DMPO was used as hydroxyl radical ($\cdot\text{OH}$) spin trapping agent and its concentration was 100 mM. The catalyst was suspended in DMPO aqueous solution. After UV irradiation for 5 min, the sample was taken very quickly and analyzed. ESR spectroscopy was measured under the following conditions: microwave power = 18.7 mW, microwave frequency = 9.418 GHz, center field = 340.1 mT, modulation frequency = 100 kHz, and sweep time = 2 min.

Catalytic performance

The photocatalytic degradation of MV was carried out *via* the addition of 50 mg of catalyst into 50 mL of 25 ppm MV dye solution. The UV irradiation was provided by a 20 W UV lamp (Hangzhou Lijing Lighting Co., Ltd., China) with 365 nm wavelength radiation and an intensity of 1100 $\mu\text{W cm}^{-2}$. The reactor was placed such that the sample was perpendicular to the UV light source at a distance of 10 cm. Each suspension prepared was magnetically stirred at 25 ± 2 °C in the dark for 30 min such that adsorption–desorption equilibrium of the MV dye on the catalyst surface was achieved. After 1 h of UV irradiation, 2 mL of the suspension was withdrawn. The change in the MV concentration was monitored using a UV-vis spectrophotometer (Hach, USA) at a wavelength of 584 nm.

$$\text{Degradation efficiency (\%)} = \left(\frac{A_0 - A}{A_0} \right) \times 100,$$

where A_0 is the MV concentration after adsorption equilibrium and before UV irradiation, and A is the MV concentration after irradiation.

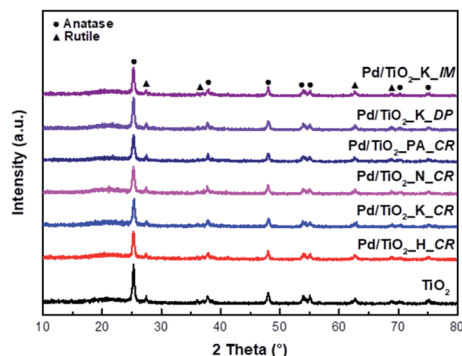


Fig. 1 XRD patterns of TiO₂ support and Pd/TiO₂ catalysts prepared by different Pd precursors and preparation methods.

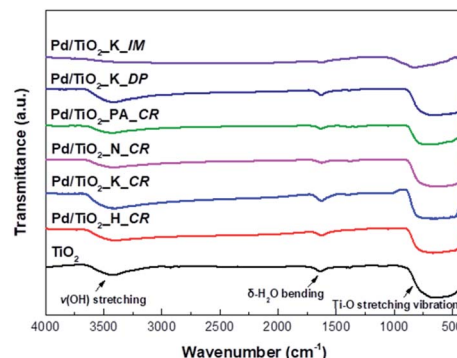


Fig. 3 FT-IR spectra of TiO₂ support and Pd/TiO₂ catalysts.

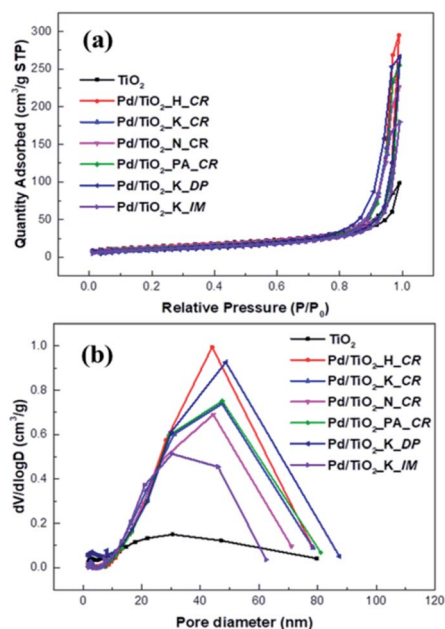


Fig. 2 N₂ adsorption-desorption curve (a) and pore size distribution (b) of TiO₂ support and Pd/TiO₂ catalysts.

Results and discussion

Catalyst characterization

Fig. 1 presents the XRD patterns of the Pd/TiO₂ catalysts prepared using different Pd precursors and preparation

methods. Pristine TiO₂ and Pd/TiO₂ exhibited distinct peaks of the anatase phase at 25.60°, 38.03°, 48.29°, 53.94°, 55.05°, 62.66°, and 68.93° corresponding to the Miller indices (101), (004), (105), (211), (204), (116), and (215), respectively.

Additionally, the XRD peaks of the rutile phase were observed at 27.45°, 36.09°, and 54.33° corresponding to the Miller indices (110), (101), and (111), respectively.¹⁴ In contrast, a decrease in intensity at $2\theta = 25.60^\circ$ was observed after the addition of Pd. This decrease was attributed to the presence of Pd atoms, which functioned as impurities or adatoms, resulting in a lower degree of crystallinity. Additionally, there were no distinct XRD peaks of Pd. This was probably because the Pd atoms were located in the bulk TiO₂ crystals.

Fig. 2 shows the N₂ adsorption-desorption isotherms of bare TiO₂ and the Pd/TiO₂ catalysts. According to the IUPAC classification, the adsorption isotherm of bare TiO₂ was of type H4 and indicated slit-like pores. The adsorption-desorption isotherms of the Pd/TiO₂ catalysts prepared changed into that of type H1 hysteresis and exhibited narrow distributions of relatively uniform mesopores. The BET surface areas, pore sizes, and pore volumes of the support and the catalysts prepared are listed in Table 1. The BET surface area of Pd/TiO₂ decreased because the pores of TiO₂ were filled with the NaOH used to adjust the pH values as well as the Pd nanoparticles.

However, the pore size and pore volume calculated using the Barrett-Joyner-Halenda (BJH) model increased. The NaOH used as a precipitating agent blocked the pores and was then deposited on the outer surface of the TiO₂ support.¹⁵ The BET

Table 1 Textural properties of TiO₂ support and the catalysts prepared by different Pd precursors and preparation methods

Samples	Precursors	Preparation methods	S_{BET} (m ² g ⁻¹)	V_{meso} (cm ³ g ⁻¹)	V_{micro}^d (cm ³ g ⁻¹)	D_p (nm)
TiO ₂			51.21	0.131	0.019	12.56
Pd/TiO ₂ _H_CR	H ₂ PdCl ₄ (H)	CR ^a	50.10	0.436	0.019	33.58
Pd/TiO ₂ _K_CR	K ₂ PdCl ₄ (K)	CR	42.86	0.380	0.015	28.70
Pd/TiO ₂ _N_CR	Na ₂ PdCl ₄ (N)	CR	49.32	0.330	0.018	27.88
Pd/TiO ₂ _PA_CR	Pd(NH ₃) ₄ Cl ₂ ·H ₂ O (PA)	CR	45.32	0.376	0.017	29.46
Pd/TiO ₂ _K_DP	K ₂ PdCl ₄ (K)	DP ^b	31.63	0.399	0.014	25.84
Pd/TiO ₂ _K_IM	K ₂ PdCl ₄ (K)	IM ^c	39.63	0.263	0.015	24.04

^a CR: chemical reduction. ^b DP: deposition-precipitation. ^c IM: impregnation method. ^d Micropore volume calculated by the Horvath-Kawazoe (HK) method.



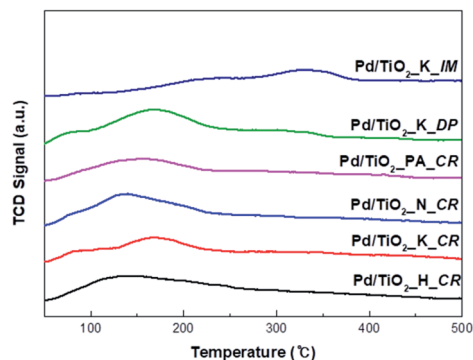


Fig. 4 CO-TPD spectra of Pd/TiO₂ catalysts (catalysts heating from 40 to 500 °C with heating rate of 5 °C min⁻¹).

Table 2 CO chemisorption data of the prepared Pd/TiO₂ catalysts

Catalysts	Metal dispersion (%)	Metallic surface area (m ² g ⁻¹ of metal)	Crystallite size (nm)
Pd/TiO ₂ _H_CR	8.01	35.70	14.00
Pd/TiO ₂ _K_CR	11.16	46.70	10.04
Pd/TiO ₂ _N_CR	5.14	22.89	21.81
Pd/TiO ₂ _PA_CR	0.74	3.31	151.03
Pd/TiO ₂ _K_DP	12.42	55.37	9.01
Pd/TiO ₂ _K_IM	3.80	16.93	29.48

surface area of the Pd/TiO₂_K_IM catalyst drastically decreased as its pores collapsed during calcination.

The FT-IR analysis was conducted to confirm the various functional groups present in the TiO₂ support and Pd/TiO₂ catalysts and the results are presented in Fig. 3. The FT-IR spectra was derived in the range 4000–400 cm⁻¹. There were broad bands at 3700–3400 cm⁻¹ and 750–520 cm⁻¹, indicating ν(OH) stretching and Ti–O stretching vibration, respectively. The weak bands at 1700 cm⁻¹ corresponded to δ-H₂O bending. In the case of Pd/TiO₂_K_IM, the band intensities at all wavenumbers decreased owing to the collapse of its pores during calcination.

The CO-TPD profiles of the catalysts prepared using different Pd precursors and preparation methods are shown in Fig. 4. The CO-TPD intensity varied with the amount of active sites available for CO adsorption. Two shoulder CO desorption peaks at approximately 80 °C and 170 °C were observed for Pd/TiO₂_K_CR and Pd/TiO₂_K_DP, respectively. Desorption peaks corresponding to lower dispersion and larger crystalline size were exhibited at higher temperatures ($T_{\text{desorption}} > 227$ °C) because of the lower Pd–CO bonding energy.^{14,15} Rieck *et al.* ascribed peaks at low temperatures ($T_{\text{desorption}} < 327$ °C) and high temperatures ($T_{\text{desorption}} > 327$ °C) to linear-bonded CO and bridge-bonded CO, respectively.¹⁸ Another study showed that the desorption of CO bound in the lower coordination sites on smaller Pd clusters occurred at lower temperatures owing to the weak intensity of the CO–Pd interaction.^{16,17} The weak desorption peak of Pd/TiO₂_PA_CR shifted to a higher temperature

(approximately 580 °C), which was assigned to the strong adsorption of CO and low metal dispersion. Consequently, the intensities of the TPD peaks were ascribed to two aspects: (i) influence of Pd particle size, and (ii) amount of linear-bonded CO species.

The results of CO chemisorption are given in Table 2. The Pd dispersion of the catalysts synthesized varied from 0.74% to 12.42% depending on the nature of the precursor salt and the preparation method. The degree of dispersion using different Pd precursors followed the trend Pd/TiO₂_K_CR > Pd/TiO₂_H_CR > Pd/TiO₂_N_CR > Pd/TiO₂_PA_CR. Kettemann *et al.* revealed that Pd chloride precursors in aqueous solutions were mainly present in the form of [PdCl₄]²⁻ and [PdCl₃(H₂O)]⁻, which reacted with NaOH to form Pd(OH)₂.¹⁹ It was further determined that Pd(OH)₂ had strong interactions with the –OH groups present on the surface of the support, leading to higher Pd dispersion. We suggested that Pd dispersion was related to the formation rate of Pd(OH)₂. When the CR method was employed in the present work, enhanced impregnation was achieved using the K₂PdCl₄ precursor whereas the lowest dispersion was attained with the impregnation of the Pd(NH₃)₄Cl₂ precursor. Monteiro *et al.* reported that higher dispersion using chloride precursors (PdCl₄²⁻) was obtained owing to the stronger interaction between the Pd anions and the –OH groups on the support.²⁰ Among K₂PdCl₄, H₂PdCl₄, and Na₂PdCl₄, K₂PdCl₄ may form polynuclear hydroxo complexes ([Pd(OH)₂]_n) more rapidly than the other two chloride precursors.^{19,21} This suggests that the smaller, hydrated Pd(OH)₂ easily precipitates into the pores on the support while Pd(NH₃)₄Cl₂ prevents the bulkier Pd²⁺ ion complexes from being deposited inside the pores. In addition, the Pd dispersion and crystallite size vary evidently with the preparation method. The dispersion of Pd/TiO₂_K_CR (approximately 11%) and that of Pd/TiO₂_K_DP (approximately 12%) were not significantly different. We supposed that the nucleation and growth rate of the Pd particles *via* ion exchange between the charged surface and Pd²⁺ ions in the CR and DP methods were similar.

As shown in Fig. 5, field emission-transmission electron microscopy (FE-TEM) images were used to confirm the Pd particle sizes and distributions of the Pd/TiO₂ catalysts prepared using different Pd precursors and preparation methods. The average Pd particle size was calculated based on a count of approximately 200 nanoparticles. When the catalysts were prepared *via* the CR method with different types of Pd precursors, the Pd particle size and distribution were influenced by the nature of the precursor. The average particle sizes of Pd/TiO₂_K_CR and Pd/TiO₂_N_CR were 2.1 nm and 3.5 nm, respectively. However, Pd/TiO₂_PA_CR had the largest particle size and broadest Pd size distribution. This was because the ammoniacal salt had a weaker precursor–support interaction compared with those of the nitrate and chloride precursors, which, combined with its bulky size, prevented deeper penetration into the micropores. Among the Pd/TiO₂_K catalysts prepared *via* the three preparation methods, Pd/TiO₂_K_IM exhibited the broadest Pd particles and largest particle size of 5.9 nm owing to the chromatographic effect. Fig. 5b reveals that Pd/TiO₂_K_DP had the smallest and most uniform Pd particles



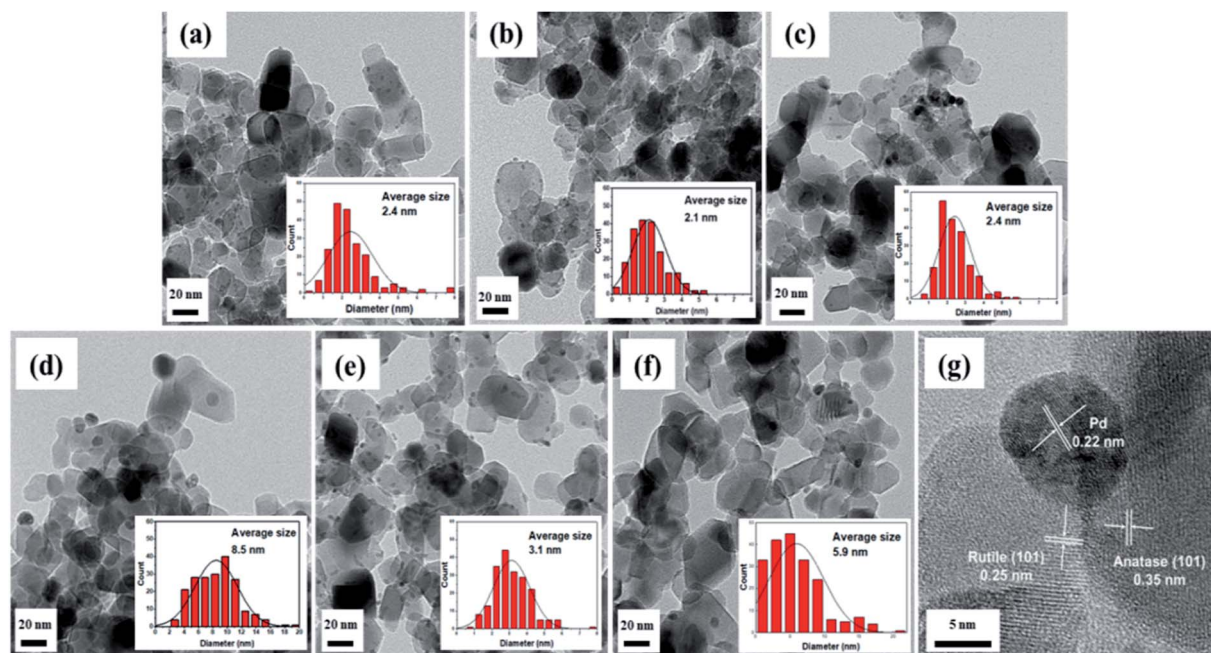


Fig. 5 FE-TEM images and Pd particle size distribution of Pd/TiO₂ catalysts: (a) Pd/TiO₂_H_CR, (b) Pd/TiO₂_K_CR, (c) Pd/TiO₂_N_CR, (d) Pd/TiO₂_PA_CR, (e) Pd/TiO₂_K_DP, and (f) Pd/TiO₂_K_IM and a HR-TEM image of (g) Pd/TiO₂_K_CR.

in agreement with the CO chemisorption results. The Pd particle size increased with Pd dispersion.

Fig. 6 and Table 3 show that the Pd 3d_{5/2} peak in the Pd/TiO₂_K_CR spectrum is deconvoluted into two peaks observed at 333.4–334.9 eV (Pd⁰) and 335.8–336.2 eV (Pd²⁺), respectively.²²

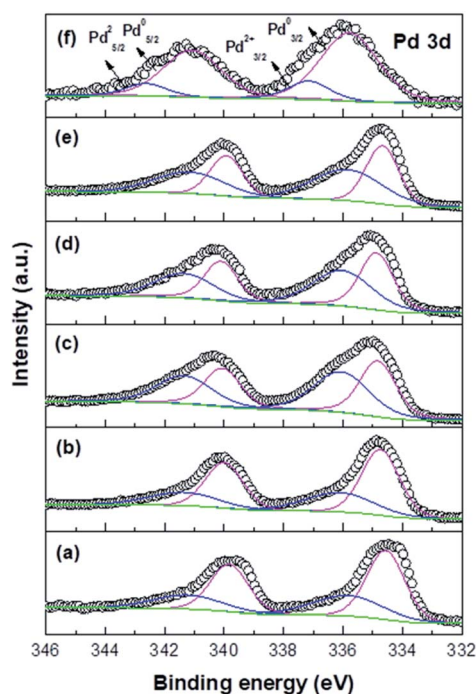


Fig. 6 XPS spectra of Pd/TiO₂ catalysts: (a) Pd/TiO₂_PA_CR, (b) Pd/TiO₂_N_CR, (c) Pd/TiO₂_H_CR, (d) Pd/TiO₂_K_CR, (e) Pd/TiO₂_K_DP, and (f) Pd/TiO₂_K_IM.

Despite the presence of a reducing agent, the Pd nanoparticles supported on TiO₂ were not completely reduced owing to the strong interaction between them. The XPS results indicated that the binding energies (BEs) of the catalysts with higher dispersion shifted positively, which exhibited higher Pd/Ti atomic ratio. On the other hand, the peaks of the catalysts with lower dispersion exhibited lower Pd/Ti atomic ratio. A good correlation was observed between the BE values and the dispersion of Pd measured *via* CO chemisorption. Moreover, the Pd²⁺/Pd⁰ ratio of each catalyst was compared. In the case of the Pd/TiO₂_K_DP and Pd/TiO₂_K_CR catalysts with higher Pd dispersion, the Pd 3d_{5/2} peaks shifted to higher BE and exhibited not only the highest Pd/Ti atomic ratio but also the highest Pd²⁺/Pd⁰ ratio. However, the Pd/Ti atomic ratio of Pd/TiO₂_PA_CR with the lowest Pd dispersion was much lower than that of Pd/TiO₂_K_DP. The Pd 3d_{5/2} BE of Pd/TiO₂_PA_CR was exhibited at 334.5 eV and 335.7 eV and the Pd⁰ peak area was much larger

Table 3 Binding energies (BEs) of Pd 3d_{5/2} and Pd/Ti atomic ratio of Pd/TiO₂ catalysts

Catalysts	BEs of Pd 3d _{5/2} (eV)		Atomic ratio	
	Pd ⁰	Pd ²⁺	Pd ²⁺ /Pd ⁰	Pd/Ti
Pd/TiO ₂ _H_CR	334.9	336.0	1.11	0.077
Pd/TiO ₂ _K_CR	334.8	336.1	1.10	0.079
Pd/TiO ₂ _N_CR	334.7	336.1	0.53	0.056
Pd/TiO ₂ _PA_CR	334.5	335.7	0.54	0.040
Pd/TiO ₂ _K_DP	334.7	335.9	1.14	0.079
Pd/TiO ₂ _K_IM	335.8	337.2	0.19	0.032



than the Pd^{2+} peak area. Mahata *et al.* proposed that the PA precursor has four ligands with NH_3 , which act as a reducing agent and facilitate the reduction of the Pd^{2+} ions.²³ We suggested that the chemical state of Pd was influenced by the formation rate of $\text{Pd}(\text{OH})_2$ as well as the intensity of the Pd–O–Ti chemical bonding.

When the Pd–O–Ti bond was formed, electrons were transferred from Pd to Ti at the Pd–O–Ti interface, forming the Pd^{2+} cationic species.²⁴ The XPS results revealed that the shift in the Pd $3d_{5/2}$ BE was influenced not only by the Pd crystalline size but also by the intensity of the precursor–support interaction. We confirmed that stronger interaction caused a positive shift in the Pd $3d_{5/2}$ BE. The Pd chemical states of the catalysts prepared *via* several methods are listed in Table 3. The XPS spectrum of Pd/TiO₂_K_IM displayed two peaks at 335.8 eV and 337.2 eV, which were attributed to the metallic Pd and PdCl_2 moieties from the Pd precursor, respectively. This electronic state was clearly different than those of the catalysts prepared *via* the DP and CR methods.

The Tauc plots of the Pd/TiO₂ catalysts were converted using the Kubelka–Munk method, as shown in Fig. S1.† The Tauc plot equation was used:

$$\alpha h\nu = A(h\nu - E_g)^n,$$

where α is the absorption coefficient, A is a constant, $h\nu$ is the photon energy, and E_g is the band gap. When $n = 1/2$, the direct band gap can be measured using the Tauc equation.²⁵

The direct band gap energy of each catalyst was estimated using the Tauc plot. The band gaps of all the Pd/TiO₂ catalysts prepared were narrower than that of pristine TiO₂, previously reported to be 3.2 eV.^{26,27} The band gaps of all the catalysts synthesized were in the range 2.88–3.03 eV. In other words, the catalysts absorbed visible light of wavelength 400–600 nm, resulting in the excitation of electrons in the valence band (VB) to the conduction band (CB) with lower energy. The band gap of Pd/TiO₂_PA_CR was slightly lower than those of the catalysts synthesized using other Pd precursors. According to the quantum confinement theory, the band gap energy decreases with increase in nanoparticle size.^{28,29} However, Pd/TiO₂_K_IM had a slightly higher band gap of 3.03 eV compared with those of the other catalysts. This might have been caused by the presence of the PdCl_2 moieties, as discerned from the XPS results. Sivaraman *et al.* reported that Cl atoms as anionic dopants increased the band gap values and enabled abundant absorption of light in the shorter wavelength spectra.³⁰ Thus, these UV-vis spectra results demonstrated that the band gap was influenced by the nanoparticle size and dopant state.

In order to identify the generation of the reactive oxygen species (ROS), the ESR spin trap with DMPO was performed.³¹ Fig. 7 displays the ESR spectra of the DMPO– $\cdot\text{OH}$ adducts under UV irradiation for 5 min in the presence of Pd/TiO₂ catalysts. DMPO aqueous solution was selected as the spin trapping agent of hydroxyl radicals. As shown in Fig. 7, the four peaks with 1 : 2 : 2 : 1 intensity ratio were clearly observed except for Pd/TiO₂_PA_CR under UV illumination. The ESR signals of Pd/TiO₂_K_CR had the strongest intensities than other catalysts,

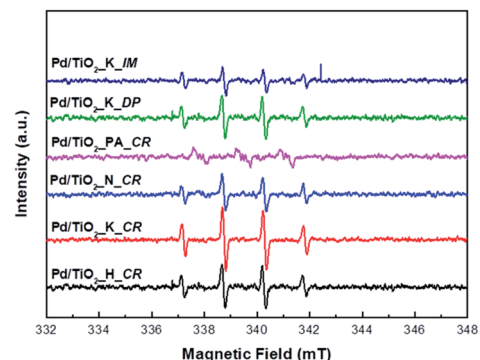


Fig. 7 ESR spectra of the $\cdot\text{OH}$ radical adduct trapped by DMPO over the prepared Pd/TiO₂ catalysts. All the spectra were measured after 5 min of UV light irradiation.

which can generate more $\cdot\text{OH}$ radicals. This is ascribed to its smallest Pd particle size, leading to facilitate the rapid diffusion of the photoinduced carriers and reduce the recombination of the carriers. Thus, more $\cdot\text{OH}$ radicals could be formed by more electrons and holes and this result was consistent with the photocatalytic activity.

Catalytic performance

The catalytic performance of the Pd/TiO₂ catalysts prepared using different Pd precursors and preparation methods was evaluated based on their photocatalytic degradation of MV under UV irradiation. Fig. 8a shows the comparative decolorization of MV by all the catalysts in the dark and under UV irradiation.

In the dark, the MV concentration slightly decreased in all the cases because of its adsorption on the surfaces of the catalysts. While Pd/TiO₂_K_DP showed the least absorption of 17% in the dark, Pd/TiO₂_PA_CR revealed the highest absorption of 26%. The increased absorption could be due to its surface charge. Methyl violet is a cationic dye classified as a Lewis acid and can easily adsorb onto negatively charged surfaces.³² With the lower $\text{Pd}^{2+}/\text{Pd}^0$ of Pd/TiO₂_PA_CR, it may be greatly absorb MV molecules due to its less repulsive interaction between MV molecules and the surface of the catalyst.

In Fig. 8, a remarkable improvement in degradation was observed under UV irradiation. The photocatalytic degradation rates under UV irradiation followed the trend Pd/TiO₂_K_DP < Pd/TiO₂_PA_CR < Pd/TiO₂_K_IM < Pd/TiO₂_H_CR < Pd/TiO₂_N_CR < Pd/TiO₂_K_CR. Although Pd dispersion of Pd/TiO₂_K_CR (11.16%) had similar to Pd/TiO₂_K_DP (12.42%), Pd/TiO₂_K_CR showed the largest rate of reaction constant (k) of 0.02191 min^{−1} and 2.03 times higher than Pd/TiO₂_K_DP. This could be that Pd/TiO₂_K_DP had the lowest specific surface area and highest $\text{Pd}^{2+}/\text{Pd}^0$ ratio, resulting in lower absorption and mass transfer of MV molecules.³³ Generally, the photocatalytic activity depends on the particle size of the metal, band gap, mesoporous volume, and surface area. Among the catalysts prepared using the H, K, and N precursors, Pd/TiO₂_N_CR had the lowest activity owing to low Pd dispersion and mesopore volume. It is known that catalytic activity is additionally



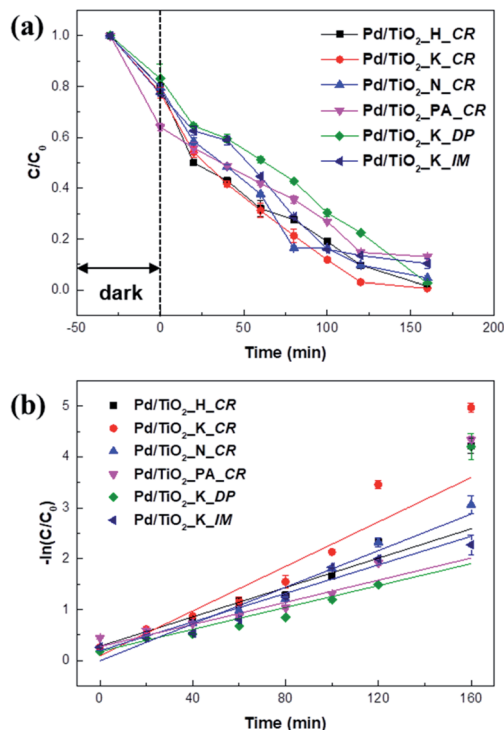


Fig. 8 Photocatalytic activity of Pd/TiO₂ catalysts for photo-degradation of MV in dark and under UV light irradiation (a) and first-order fitting curves of the catalysts (b).

influenced by the dispersion of the metal nanoparticles.^{34–36} The low activity of Pd/TiO₂_N_CR was attributed to its lower Pd dispersion and mesopore volume, which hindered charge transfer between the Pd nanoparticles and TiO₂ support and mass transport.^{37,38}

In the present work, the adsorption in the dark relied on the Pd²⁺/Pd⁰ ratio due to the electrostatic repulsion with the cationic dye. Furthermore, we found that the photodegradation performance under UV illumination were significantly dependent on Pd dispersion, Pd particle size, and specific surface area. Therefore, we can assume that the Pd²⁺/Pd⁰ ratio on the surface and the band gap are crucial factors influencing the photocatalytic degradation of MV.

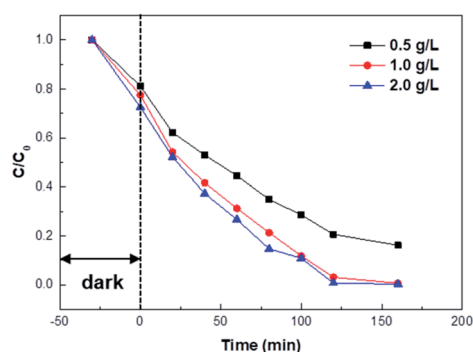
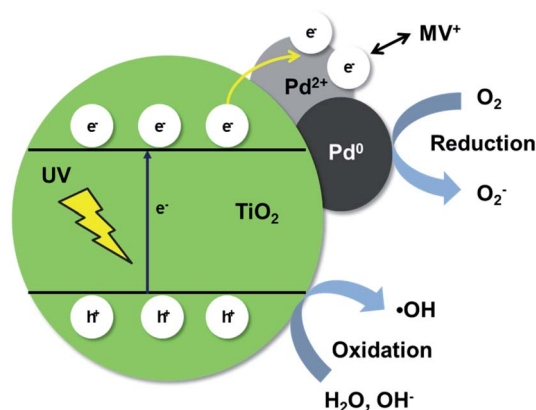


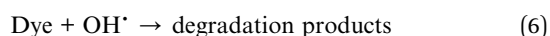
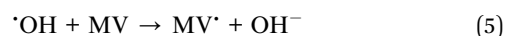
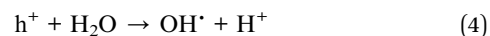
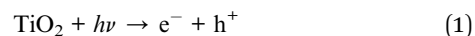
Fig. 9 Photocatalytic degradation of MV at different catalyst amounts of Pd/TiO₂_K_CR. C is the absorbance of MV at 584 nm.



Scheme 1 A proposed mechanism for photocatalytic degradation of MV over Pd/TiO₂ catalysts.

Fig. 9 presents the effect of 5 wt% Pd/TiO₂_K_CR catalyst amounts on the photocatalytic activity. To investigate the optimal catalyst amount, the catalyst amounts were varied from 0.5 g L⁻¹ to 2.0 g L⁻¹. The results revealed that the photocatalytic activity remarkably enhanced from 0.5 g L⁻¹ to 1.0 g L⁻¹. When the catalyst amount was 2.0 g L⁻¹, the degradation curve was similar to 1.0 g L⁻¹. 160 min was taken to sufficiently achieve the decolorization efficiency of 99.67%.

Based on the above results, a suggested mechanism of the photocatalytic degradation of MV by the Pd/TiO₂ catalysts is depicted in Scheme 1 and represented by the following scheme.



Water molecules compete with the MV dye molecules for adsorption onto the catalyst in the solution. Under UV irradiation, the electrons of TiO₂ are elevated from the VB to the CB and holes are generated in the VB. The photoinduced electrons then migrate to the Pd nanoparticles working as scavengers, which act like electron traps and reduce the recombination of electron-hole pairs.^{38–40} The Pd²⁺ species on the catalyst are then reduced by the photoinduced electrons upon irradiation, which diminishes electrostatic repulsion. The free OH⁻ on the surface of TiO₂ captures the holes in the VB of TiO₂ to produce the ·OH radical.

A possible degradation pathways of MV are the destruction of MV chromophore structures and N-de-methylation.^{41,42} The produced ·OH radical attack on MV and the cationic radical MV⁺. Then, MV⁺ was continuously degraded via attack of ·OH

radical and *N*-de-methylation, resulting in *N,N*-dimethylaminobenzene, aminobenzene, acetamide, 2-propenoic acid, etc. These are further mineralized into CO_3^{2-} and NO_3^{2-} .

Conclusions

We have shown that Pd dispersion and catalytic performance are remarkably affected by the type of Pd species in solution and catalyst preparation method. The catalytic performance was tested based on the photocatalytic degradation of MV. In particular, higher dispersion of Pd was obtained on the Pd/TiO₂ catalyst prepared *via* the CR method with the K precursor compared with those achieved using other Pd precursors. The catalyst obtained *via* deposition-precipitation, *i.e.*, Pd/TiO₂-K_DP, exhibited the highest dispersion of 12.42% among those prepared *via* the three different methods. This was ascribed to the formation of Pd(OH)₂, which exhibited strong interaction with the -OH group as well as a strong chemical bond of Pd-O-Ti. Further, the Pd²⁺/Pd⁰ ratio increased with Pd dispersion. The photocatalytic degradation of MV was chosen to evaluate the photocatalytic activities of Pd/TiO₂ catalysts. Pd/TiO₂-PA_CR showed the highest adsorption in the absence of UV light due to lower Pd²⁺/Pd⁰ ratio. It was found that high Pd²⁺/Pd⁰ ratio in dark condition adversely affected the absorption of MV owing to electrostatic repulsion between MV⁺ and metal nanoparticles. However, the Pd dispersion and the specific surface area played a key role in the photocatalytic activity under UV irradiation. Pd/TiO₂-K_CR with higher Pd dispersion showed the highest photocatalytic activity and reaction rate of 0.0212 min⁻¹.

Conflicts of interest

There are no conflicts to declare.

Acknowledgements

This work was supported by the Technology Innovation Program (20000126) funded by the Ministry of Trade, Industry & Energy (MOTIE, Korea), Korea Institute of Industrial Technology through Research and Development (EO-20-0014) and Ulsan Metropolitan City (IZ-20-0540).

References

- 1 J. S. Wu, C. H. Liu, K. H. Chu and S. Y. Suen, *J. Membr. Sci.*, 2008, **309**, 239–245.
- 2 R. Kant, *Nat. Sci.*, 2012, **04**, 22–26.
- 3 T. A. Nguyen and R. S. Juang, *Chem. Eng. J.*, 2013, **219**, 109–117.
- 4 S. Chen, J. Zhang, C. Zhang, Q. Yue, Y. Li and C. Li, *Desalination*, 2010, **252**, 149–156.
- 5 M. Solís, A. Solís, H. I. Pérez, N. Manjarrez and M. Flores, *Process Biochem.*, 2012, **47**, 1723–1748.
- 6 A. Hethnawi, N. N. Nassar, A. D. Manasrah and G. Vitale, *Chem. Eng. J.*, 2017, **320**, 389–404.
- 7 C. K. C. Araújo, G. R. Oliveira, N. S. Fernandes, C. L. P. S. Zanta, S. S. L. Castro, D. R. da Silva and C. A. Martínez-Huitle, *Environ. Sci. Pollut. Res.*, 2014, **21**, 9777–9784.
- 8 J. Wu, S. Lu, D. Ge, L. Zhang, W. Chen and H. Gu, *RSC Adv.*, 2016, **6**, 67502–67508.
- 9 J. M. Walls, J. S. Sagu and K. G. Upul Wijayantha, *RSC Adv.*, 2019, **9**, 6387–6394.
- 10 M. Y. Abdelaal and R. M. Mohamed, *J. Alloys Compd.*, 2013, **576**, 201–207.
- 11 H. Khojasteh, M. Salavati-Niasari, A. Abbasi, F. Azizi and M. Enhessari, *J. Mater. Sci.: Mater. Electron.*, 2016, **27**, 1261–1269.
- 12 Z. Wu, Z. Sheng, H. Wang and Y. Liu, *Chemosphere*, 2009, **77**, 264–268.
- 13 X. Meng, Z. Li, N. Yun and Z. Zhang, *J. Nanomater.*, 2018, **2018**, 1234506.
- 14 K. K. Gupta, N. L. Singh, A. Pandey, S. K. Shukla, S. N. Upadaya, V. Mishra, P. Srivastava, N. P. Lalla and P. K. Mishra, *J. Dispersion Sci. Technol.*, 2013, **34**, 1043–1052.
- 15 H. Huang and D. Y. C. Leung, *ACS Catal.*, 2011, **1**, 348–354.
- 16 W. J. Shen, M. Okumura, Y. Matsumura and M. Haruta, *Appl. Catal., A*, 2001, **213**, 225–232.
- 17 W. E. Kaden, W. A. Kunkel, F. S. Roberts, M. Kane and S. L. Anderson, *J. Chem. Phys.*, 2012, **136**, 204705.
- 18 J. S. Rieck and A. T. Bell, *J. Catal.*, 1987, **103**, 46–54.
- 19 F. Kettemann, M. Wuthschick, G. Caputo, R. Kraehnert, N. Pinna, K. Rademann and J. Polte, *CrystEngComm*, 2015, **17**, 1865–1870.
- 20 R. S. Monteiro, L. C. Dieguez and M. Schmal, *Catal. Today*, 2001, **65**, 77–89.
- 21 M. Turáková, M. Králik, P. Lehocký, Ľ. Pikna, M. Smrčová, D. Remeteiová and A. Hudák, *Appl. Catal., A*, 2014, **476**, 103–112.
- 22 L. M. Esteves, M. H. Brijaldo and F. B. Passos, *J. Mol. Catal. A: Chem.*, 2016, **422**, 275–288.
- 23 N. Mahata and V. Vishwanathan, *J. Catal.*, 2000, **196**, 262–270.
- 24 R. Gopinath, N. Seshu Babu, J. Vinod Kumar, N. Lingaiah and P. S. Sai Prasad, *Catal. Lett.*, 2008, **120**, 312–319.
- 25 E. Sanchez and T. Lopez, *Mater. Lett.*, 1995, **25**, 271–275.
- 26 J. F. Guayaquil-Sosa, B. Serrano-Rosales, P. J. Valadés-Pelayo and H. de Lasa, *Appl. Catal., B*, 2017, **211**, 337–348.
- 27 K. I. Omoniyi, A. Aroh, C. Gimba, H. Abba and M. Yilleng, *J. Sci. Technol.*, 2018, **10**, 60–66.
- 28 X. Zhang, J. He, W. Chen, C. Wang, C. Zheng, J. Lin, X. Zheng and F. Huang, *RSC Adv.*, 2014, **4**, 34288–34293.
- 29 E. O. Chukwuocha, M. C. Onyeaju and T. S. T. Harry, *World J. Condens. Matter Phys.*, 2012, **2**, 96–100.
- 30 T. Sivaraman, V. Narasimman, V. S. Nagarethinam and A. R. Balu, *Prog. Nat. Sci.: Mater. Int.*, 2015, **25**, 392–398.
- 31 P. Shao, S. Yu, X. Duan, L. Yang, H. Shi, L. Ding, J. Tian, L. Yang, X. Luo and S. Wang, *Environ. Sci. Technol.*, 2020, **54**, 8464–8472.
- 32 H. Puchler, S. N. Meloan and M. Spencer, *Histochemistry*, 1985, **82**, 301–306.
- 33 F. Amano, K. Nogami, M. Tanaka and B. Ohtani, *Langmuir*, 2010, **26**, 7174–7180.



- 34 L. Hou, M. Zhang, Z. Guan, Q. Li and J. Yang, *J. Nanopart. Res.*, 2018, **20**, 60.
- 35 N. M. Gupta, S. V. Awate, A. A. Belhekar, S. V. Bhagwat and R. Kumar, *Int. J. Photoenergy*, 2008, **2008**, 789149.
- 36 M. Y. Byun, D. W. Park and M. S. Lee, *Catal. Today*, 2020, **352**, 88–94.
- 37 I. Majeed, U. Manzoor, F. K. Kanodarwala, M. A. Nadeem, M. A. Nadeem, E. Hussain, H. Ali, A. Badshah and J. A. Stride, *Catal. Sci. Technol.*, 2018, **8**, 1183–1193.
- 38 B. Fang, Y. Xing, A. Bonakdarpour, S. Zhang and D. P. Wilkinson, *ACS Sustainable Chem. Eng.*, 2015, **3**, 2381–2388.
- 39 J. Gomes, A. Lopes, K. Bednarczyk, M. Gmurek, M. Stelmachowski, A. Zaleska-Medynska, M. Quinta-Ferreira, R. Costa, R. Quinta-Ferreira and R. Martins, *ChemEngineering*, 2018, **2**, 4.
- 40 U. I. Gaya and A. H. Abdullah, *J. Photochem. Photobiol., C*, 2008, **9**, 1–12.
- 41 Y.-H. B. Liao, J. X. Wang, J.-S. Lin, W.-H. Chung, W.-Y. Lin and C.-C. Chen, *Catal. Today*, 2011, **174**, 148–159.
- 42 A. Bhattacharjee, M. Ahmaruzzaman, T. B. Devi and J. Nath, *J. Photochem. Photobiol., A*, 2016, **325**, 116–124.

